Rotation Curve of the Milky Way from Classical Cepheids

Przemek Mróz[1] , Andrzej Udalski[1], Dorota M. Skowron[1], Jan Skowron[1] , Igor Soszyński[1], Paweł Pietrukowicz[1] ,
Michał K. Szymański[1], Radosław Poleski[1,2] , Szymon Kozłowski[1] , and Krzysztof Ulaczyk[1,3]

[1] Warsaw University Observatory, Al. Ujazdowskie 4, 00-478 Warszawa, Poland; pmroz@astrouw.edu.pl
[2] Department of Astronomy, Ohio State University, 140 West 18th Avenue, Columbus, OH 43210, USA
[3] Department of Physics, University of Warwick, Coventry CV4 7AL, UK

Abstract

Flat rotation curves of spiral galaxies are considered as an evidence for dark matter, but the rotation curve of the Milky Way is difficult to measure. Various objects were used to track the rotation curve in the outer parts of the Galaxy, but most studies rely on incomplete kinematical information and inaccurate distances. Here, we use a sample of 773 Classical Cepheids with precise distances based on mid-infrared period–luminosity relations coupled with proper motions and radial velocities from *Gaia* to construct the accurate rotation curve of the Milky Way up to the distance of ∼20 kpc from the Galactic center. We use a simple model of Galactic rotation to measure the rotation speed of the Sun $\Theta_0 = 233.6 \pm 2.8$ km s^{-1}, assuming a prior on the distance to the Galactic center $R_0 = 8.122 \pm 0.031$ kpc from the GRAVITY Collaboration. The rotation curve at Galactocentric distances $4 \lesssim R \lesssim 20$ kpc is nearly flat with a small gradient of -1.34 ± 0.21 km s^{-1} kpc^{-1}. This is the most accurate Galactic rotation curve at distances $R > 12$ kpc constructed so far.

Key words: Galaxy: fundamental parameters – Galaxy: kinematics and dynamics – stars: kinematics and dynamics – stars: variables: Cepheids

1. Introduction

Flat rotation curves of spiral galaxies provide evidence for dark matter (Rubin et al. 1980) or even "new physics" (Milgrom 1983), but the rotation curve of our Galaxy is notoriously difficult to measure, especially in the outer parts of the Milky Way. The most popular approach, the tangent-point method (e.g., Burton & Gordon 1978; Clemens 1985; Fich et al. 1989; Sofue et al. 2009; McClure-Griffiths & Dickey 2016), based on radio and mm observations of common molecules (H I or CO), allows measuring the rotation curve within the solar orbit, although it is unreliable in the central regions of the Galaxy (Chemin et al. 2015). The rotation curve outside the solar orbit can be measured with known distances and velocities of some tracers: H II regions (Fich et al. 1989; Brand & Blitz 1993), Cepheids (Pont et al. 1994, 1997; Metzger et al. 1998; Kawata et al. 2018), open clusters (Hron 1987), or planetary nebulae (Durand et al. 1998), but the current uncertainties are considerable (see Figure 1 of Sofue et al. 2009), mostly because of poorly known distances. Such an approach is prone to systematic errors, as usually only one component of the velocity vector (radial or tangential) is known, and the circular rotation is assumed. As radial velocities and proper motions are measured relative to the Sun, both methods require independent information about the velocity of the Sun and distance to the Galactic center. See Bhattacharjee et al. (2014), Pato & Iocco (2017), Russeil et al. (2017), and references therein for recent data compilations.

A novel approach for constructing the Galactic rotation curve is presented by Reid et al. (2009, 2014) and Honma et al. (2012), who have measured accurate trigonometric parallaxes, proper motions, and radial velocities of about 100 high-mass star-forming regions. They use the three-dimensional velocity information to calculate the rotation curve and to simultaneously estimate the velocity and location of the Sun. Their

sample is relatively small and most of objects they analyze are located in the northern part of the Galactic disk, which may introduce some bias. The local rotation curve was published by the Gaia Collaboration et al. (2018b), who used the second *Gaia* data release (*Gaia* DR2) to study motions of nearby stars, but their parallaxes are accurate in the solar neighborhood, within 2–3 kpc of the Sun.

Recently, Udalski et al. (2018) presented the new Optical Gravitational Lensing Experiment (OGLE) Collection of Galactic Cepheids containing 1426 Classical Cepheids based on the survey of the Galactic plane carried out as part of the OGLE project. This data set more than doubled the number of known Galactic Cepheids. The survey covers over 2500 square degrees along the Galactic plane ($-170° < l < +40°$, $-6° < b < +3°$) and probes the Galactic disk out to its expected boundary (∼20 kpc from the Galactic center). That sample, supplemented with previously known all-sky Cepheids, was used by Skowron et al. (2018) to study the structure of the young Milky Way disk.

Here, we complement distances to Cepheids from Skowron et al. (2018) with the kinematical data (proper motions, radial velocities) to measure the three-dimensional velocities of Cepheids (Section 2). We use a simple model of Galactic rotation to measure the velocity of the Sun (Section 3) and to construct the accurate rotation curve of the Milky Way up to the Galactocentric distance of 20 kpc (Section 4).

2. Data

Skowron et al. (2018) measured accurate distances for 2177 Galactic Cepheids, using the period–luminosity relations of Wang et al. (2018) and mid-infrared light curves, which virtually removes the effects of interstellar extinction. We cross-matched Skowron et al.'s catalog with *Gaia* DR2 (Gaia Collaboration et al. 2016, 2018a) and found that the full

velocity information (proper motions and median radial velocities) is available for 832 objects.[4]

We used distances measured by Skowron et al. (2018), as *Gaia* parallaxes are not sufficiently accurate for many objects from our sample. Additionally, Riess et al. (2018) and Groenewegen (2018) showed that *Gaia* parallaxes are systematically lower than accurate non-*Gaia* parallaxes of Classical Cepheids by -0.046 ± 0.013 mas and -0.049 ± 0.018 mas, respectively. We also found a similar median offset of -0.071 ± 0.038 mas between *Gaia* and Skowron et al.'s (2018) parallaxes (we compared distances of 251 Cepheids that have parallax uncertainties smaller than 10%). The similar parallax zero-point offset, from -0.029 to -0.082 mas, was found for other tracers (see Groenewegen 2018 and references therein). Typical distance uncertainties are of a few per cent.

Known Cepheids located in binary systems[5] (Szabados 2003) were not included in the modeling. For the final models, we also removed a few objects with residual velocities at least 4σ larger than the mean, where σ is the dispersion of residuals. These can be unrecognized binary Cepheids (with incorrect *Gaia* astrometric solutions) or variables of other type that were mistaken with Cepheids. We were left with 773 objects. The radial velocities of Cepheids show variations with amplitudes up to $30 \, \mathrm{km \, s^{-1}}$ with the pulsation period (Joy 1937; Stibbs 1955). Radial velocities reported in the *Gaia* DR2 are median values of single-transit measurements. Cepheids from our sample were observed from 2 to 44 times, with a median number of seven visits. A small number of single observations is usually reflected by large error bars, although in some cases, the uncertainties may be underestimated (if the measurements happened to be collected near the same pulsation phase). Thus, for the modeling, we added in quadrature a constant value (about $14 \, \mathrm{km \, s^{-1}}$) to the reported radial velocity uncertainties.

3. Modeling

We use a simple model of circular rotation of the Milky Way. For each Cepheid, with known Galactic coordinates (longitude l and latitude b) and heliocentric distance D, we calculate the expected radial and tangential velocities and compare them with observations.

Our model has the following free parameters: R_0—distance of the Sun to the Galactic center, (U_s, V_s, W_s)—mean noncircular motion of the source in a Cartesian Galactocentric frame, $(U_\odot, V_\odot, W_\odot)$—solar motion with respect to the local standard of rest (LSR), and one to three parameters that describe the shape of the rotation curve. We follow the notation from the Appendix of Reid et al. (2009): U_i is the velocity component toward the Galactic center, V_i—along the Galactic rotation, and W_i—toward the North Galactic pole. We consider three analytical rotation curves: $\Theta(R) = \Theta_0 = \mathrm{const}$ (model 1) and $\Theta(R) = \Theta_0 + \frac{d\Theta}{dR}(R - R_0)$ (model 2), where Θ_0 and $\frac{d\Theta}{dR}$ are parameters and R is the distance to the Galactic center. The third model is based on a universal rotation curve introduced by Persic et al. (1996), which describes, in a simple way, contributions from the stellar disk and dark matter halo to the total rotation velocity. That model has three parameters: a_1—the rotation speed at the optical radius R_{opt} of the galaxy, $a_2 = R_{\mathrm{opt}}/R_0$, and a_3—the "velocity core radius" (in units

---

[4] The data, as well as the modeling code, are publicly available at ftp://ftp.astrouw.edu.pl/ogle/ogle4/ROTATION_CURVE/.
[5] http://www.konkoly.hu/CEP/intro.html

---

of R_{opt}), a_2 and a_3 define the shape of the rotation curve:

$$\Theta_d^2(x) = a_1^2 b \frac{1.97 x^{1.22}}{(x^2 + 0.78^2)^{1.43}} \qquad (1)$$

$$\Theta_h^2(x) = a_1^2 (1 - b) x^2 \frac{1 + a_3^2}{x^2 + a_3^2} \qquad (2)$$

$$\Theta(x) = \sqrt{\Theta_d^2(x) + \Theta_h^2(x)} \qquad (3)$$

$$x = R/R_{\mathrm{opt}} = (R/R_0)/a_2. \qquad (4)$$

We adopt $b = 0.72$ (Persic et al. 1996; Reid & Dame 2016).

The total velocity of the Cepheid is $(U_s, V_s + \Theta(R), W_s)$. Let β be the angle between the Sun and the source as viewed from the Galactic center (see Figure 9 of Reid et al. 2009). We rotate the velocity vector through the angle $-\beta$ and subtract the velocity of the Sun:

$$U_1 = U_s \cos\beta + (V_s + \Theta(R))\sin\beta - U_\odot, \qquad (5)$$

$$V_1 = -U_s \sin\beta + (V_s + \Theta(R))\cos\beta - V_\odot - \Theta_0, \qquad (6)$$

$$W_1 = W_s - W_0. \qquad (7)$$

The radial velocity V_r and tangential velocities in Galactic coordinates (V_l and V_b) can be calculated as follows:

$$V_l = V_1 \cos l - U_1 \sin l, \qquad (8)$$

$$V_b = W_1 \cos b - (U_1 \cos l + V_1 \sin l)\sin b, \qquad (9)$$

$$V_r = W_1 \sin b + (U_1 \cos l + V_1 \sin l)\cos b. \qquad (10)$$

We maximize the following likelihood function:

$$\ln \mathcal{L} = -\frac{1}{2} \sum_{i=1 \dots N} \sum_{j=l,b,r} \left(\frac{(V_{i,j} - V_{i,j,\mathrm{model}})^2}{\sigma_{V_{i,j}}^2 + \epsilon_j^2} + \ln(\sigma_{V_{i,j}}^2 + \epsilon_j^2) \right), \qquad (11)$$

where $\sigma_{V_{i,j}}$ is the velocity uncertainty and ϵ_l, ϵ_b, and ϵ_r are additional parameters that describe the scatter in V_l, V_b, and V_r (the scatter of residuals is much larger than the original error bars owing to the peculiar (noncircular) motion of stars).

The best-fit parameters are found by maximizing the likelihood function using the simplex approach (Nelder & Mead 1965). The uncertainties are estimated using the Markov chain Monte Carlo (MCMC) technique (Foreman-Mackey et al. 2013) and represent 68% confidence range of marginalized posterior distributions, see Table 1. As we found that the velocity of the Sun with respect to the LSR is poorly constrained by the data, we used the following Gaussian priors: $U_\odot = 11.1 \pm 1.3 \, \mathrm{km \, s^{-1}}$, $V_\odot = 12.2 \pm 2.1 \, \mathrm{km \, s^{-1}}$, and $W_\odot = 7.3 \pm 0.7 \, \mathrm{km \, s^{-1}}$ (Schönrich et al. 2010). We assumed uniform priors on other parameters.

We found that Θ_0 and R_0 are strongly correlated. Their correlation coefficient, calculated using MCMC chains, is equal to about 0.73 (Table 1). Our best estimates of $R_0 \approx 7.6$ kpc are smaller than the most accurate current measurement from the GRAVITY Collaboration ($R_0 = 8.122 \pm 0.031$ kpc; Abuter et al. 2018). Other recent determinations also favor the larger value: $R_0 = 7.93 \pm 0.14$ kpc (Chu et al. 2018) and $R_0 = 8.20 \pm 0.09$ kpc (McMillan 2017). To understand the reason of this difference, we added a Gaussian prior on R_0. We found that models with the prior on R_0 are disfavored by $2\Delta \ln \mathcal{L} = 19.4$, but most of this signal can be attributed to two stars EX Mus ($D = 17.5 \pm 0.8$ kpc, $A_K = 0.08$ mag) and V800 Aql

Table 1
Best-fit Model Parameters

| Parameter	Model 1	Model 2 Without Prior on R_0	Model 3	Model 1	Model 2 With Prior on R_0	Model 3
Θ_0 (km s^{-1})	221.3 ± 3.6	222.3 ± 3.6	221.5 ± 3.6	233.3 ± 2.6	233.6 ± 2.6	233.8 ± 2.7
$\frac{d\Theta}{dR}$ (km s^{-1} kpc^{-1})	0.0 (fixed)	-1.32 ± 0.20	...	0.0 (fixed)	-1.34 ± 0.20	...
R_0 (kpc)	7.57 ± 0.12	7.60 ± 0.11	7.56 ± 0.12	8.09 ± 0.03	8.09 ± 0.03	8.09 ± 0.03
U_s (km s^{-1})	1.3 ± 1.0	1.6 ± 1.0	1.5 ± 1.0	1.4 ± 1.0	1.7 ± 1.0	1.7 ± 1.0
V_s (km s^{-1})	-5.2 ± 2.2	-3.4 ± 2.3	-2.2 ± 2.3	-6.2 ± 2.2	-4.4 ± 2.2	-3.4 ± 2.3
W_s (km s^{-1})	1.0 ± 0.8	1.0 ± 0.8	1.0 ± 0.8	1.0 ± 0.8	1.0 ± 0.8	1.0 ± 0.8
$U_\odot$ (km s^{-1})	9.7 ± 1.0	10.0 ± 1.0	9.9 ± 1.0	9.8 ± 1.0	10.1 ± 1.0	10.1 ± 1.0
$V_\odot$ (km s^{-1})	12.1 ± 2.2	12.1 ± 2.1	12.0 ± 2.1	12.2 ± 2.1	12.3 ± 2.1	12.1 ± 2.2
$W_\odot$ (km s^{-1})	7.3 ± 0.7	7.3 ± 0.7	7.3 ± 0.7	7.3 ± 0.7	7.3 ± 0.7	7.3 ± 0.7
a_1 (km s^{-1})	...	...	222.8 ± 3.6	...	...	235.0 ± 2.8
a_2	...	...	0.88 ± 0.05	...	...	0.89 ± 0.05
a_3	...	...	1.31 ± 0.06	...	...	1.31 ± 0.06
ϵ_l (km s^{-1})	13.5 ± 0.4	13.4 ± 0.4	13.3 ± 0.4	13.8 ± 0.4	13.7 ± 0.4	13.4 ± 0.4
ϵ_b (km s^{-1})	7.6 ± 0.2	7.6 ± 0.2	7.6 ± 0.2	7.6 ± 0.2	7.6 ± 0.2	7.6 ± 0.2
ϵ_r (km s^{-1})	14.6 ± 0.5	14.3 ± 0.5	14.3 ± 0.5	14.6 ± 0.5	14.2 ± 0.5	14.2 ± 0.5
$\Omega_0 = \Theta_0/R_0$ (km s^{-1} kpc^{-1})	29.22 ± 0.33	29.25 ± 0.33	29.28 ± 0.33	28.84 ± 0.31	28.88 ± 0.31	28.92 ± 0.32
$(\Theta_0 + V_\odot)/R_0$ (km s^{-1} kpc^{-1})	30.82 ± 0.20	30.84 ± 0.19	30.88 ± 0.19	30.35 ± 0.16	30.40 ± 0.16	30.41 ± 0.16
$\Delta \ln \mathcal{L}$	0.0	21.3	35.3	0.0	21.4	34.2
ρ_{R_0,Θ_0}	0.74	0.73	0.73	0.28	0.27	0.26

Note. Model 1: flat rotation curve $\Theta(R) = \Theta_0 = $ const, model 2: linear rotation curve $\Theta(R) = \Theta_0 + \frac{d\Theta}{dR}(R - R_0)$, model 3: the universal rotation curve (Persic et al. 1996), see Equations (1)–(4). $\Delta \ln \mathcal{L}$ is the log-likelihood improvement relative to the model 1. ρ_{R_0,Θ_0} is the correlation coefficient between R_0 and Θ_0. We used the following Gaussian priors on the motion of the Sun: $U_\odot = 11.1 \pm 1.3$ km s^{-1}, $V_\odot = 12.2 \pm 2.1$ km s^{-1}, and $W_\odot = 7.3 \pm 0.7$ km s^{-1} (Schönrich et al. 2010). We consider models with and without the Gaussian prior on $R_0 = 8.112 \pm 0.031$ kpc (Abuter et al. 2018).

($D = 18.5 \pm 1.0$ kpc, $A_K = 0.24$ mag), both of which are located far from the Sun, and their distance may be affected by systematic errors (mostly the interstellar extinction A_K in the K band). If these two stars are removed from the sample, models with $R_0 = 8.122$ kpc are disfavored by only $2\Delta \ln \mathcal{L} = 8.4$. As there is a priori no reason to remove these two stars, we prefer to use models with priors on R_0.

Moreover, models without a constraint on R_0 produce the angular speed of the Sun about the Galactic center ($(\Theta_0 + V_\odot)/R_0$, see Table 1) that is in tension with the accurate measurement of the proper motion of Sgr A* (30.24 ± 0.12 km s^{-1} kpc^{-1}; Reid & Brunthaler 2004). Using the R_0 measured by the GRAVITY Collaboration removes this tension. Then, the estimated Θ_0 raises to 233.6 ± 2.6 km s^{-1} (model 2) and 233.8 ± 2.7 km s^{-1} (model 3), see Table 1.

The cumulative distribution of residuals $R_{i,j} = (V_{i,j} - V_{i,j,\text{model}})/\sqrt{\sigma_{V_{i,j}}^2 + \epsilon_j^2}$ from the best-fit model (model 2 with the prior on R_0) is shown in Figure 1. The residuals (of all three velocity components) follow the Gaussian distribution well.

We found that both linear and universal rotation curves describe that data much better than a simple constant rotation curve, with log-likelihood improvement $2\Delta \ln \mathcal{L}$ of 42.8 and 68.4, respectively. Linear and universal rotation curve models have similar maximal log-likelihoods, but the latter model is slightly preferred. This preference is mainly caused by a few Cepheids with velocities lower than 200 km s^{-1}, which are located at distances ≈ 4 kpc from the Galactic center (Figure 2). Similarly, Reid et al. (2014) found that velocities of masers closest to the Galactic center ($R \lesssim 5$ kpc) deviate from the flat
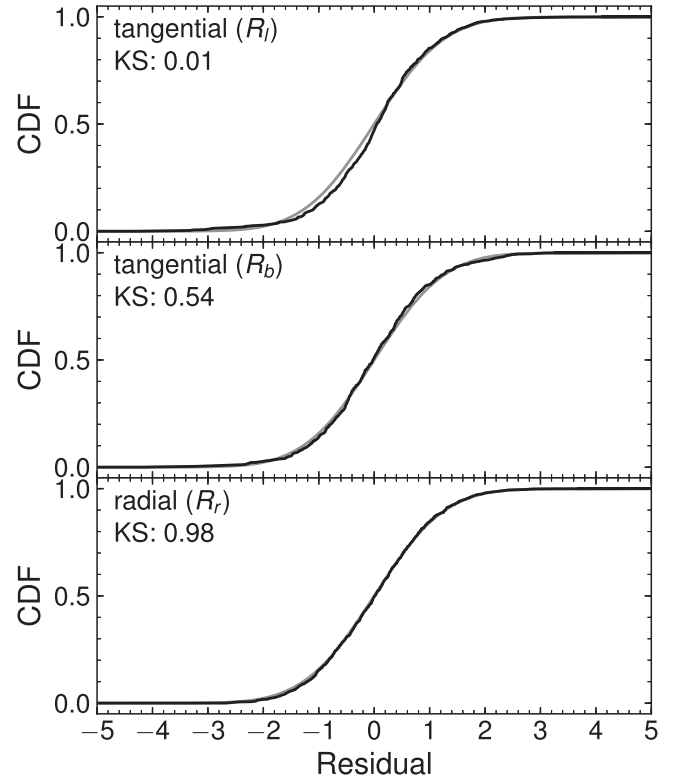
Figure 1. The black line shows the cumulative distribution of residuals from the best-fit model (model 2 with the prior on R_0). This distribution is compared to a standard Gaussian distribution, and we quote the p-value of the Kolmogorov–Smirnov (KS) test. The gray line shows the cumulative distribution function of the normal distribution.
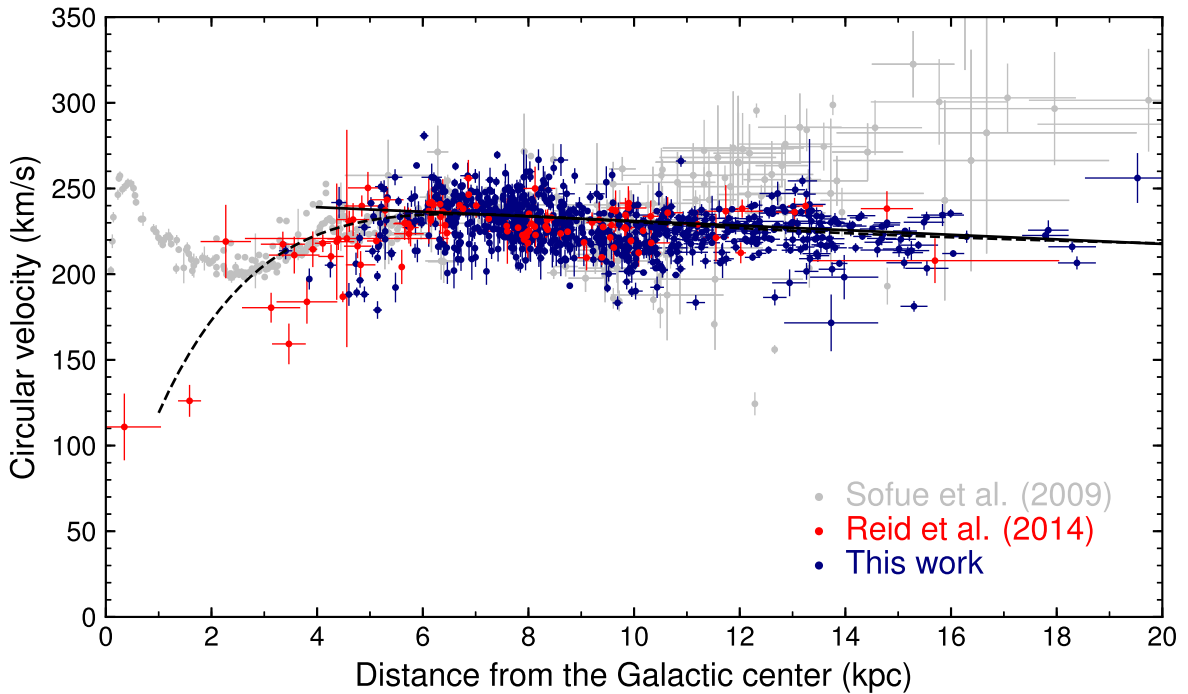
Figure 2. Rotation curve of the Milky Way for Cepheids assuming $R_0 = 8.09$ kpc and $\Theta_0 = 233.6$ km s^{-1} (model 2). Red data points represent high-mass star-forming regions (Reid et al. 2014). Gray data points are taken from Sofue et al. (2009) and are rescaled to new (R_0, Θ_0) using formula $V_{new} = V_{old} + \frac{R}{8.0}(\Theta_0 - 200)$. Solid and dashed lines show the best-fitting models (linear and universal, respectively).

rotation curve. The universal rotation curve model of Persic et al. (1996), however, does not agree with observations collected by Sofue et al. (2009) for $R \lesssim 3$ kpc (Figure 2). These measurements, obtained with the tangent-point method may be unreliable as argued by Chemin et al. (2015). The current sample of Cepheids is too small to credibly distinguish between the two models.

To assess how distance uncertainties influence the final parameters, we carried out Monte Carlo simulations. For each Cepheid, we drew a new distance from the normal distribution and repeated our modeling procedure. We conducted 100 trials, in which we found the additional spread of Θ_0 and $d\Theta/dR$ of 0.8 km s^{-1} and 0.05 km s^{-1} kpc^{-1}, respectively. We add these quantities in quadrature to the uncertainties from Table 1, finding $\Theta_0 = 233.6 \pm 2.8$ km s^{-1} and $d\Theta/dR = -1.34 \pm 0.21$ km s^{-1} kpc^{-1} for model 2.

Residuals from the best-fit models are shown in Figure 3, separately for radial, azimuthal, and vertical velocity components. Error bars of many individual objects are much lower than the scatter ($\sigma_U = 16$ km s^{-1}, $\sigma_V = 14$ km s^{-1}, $\sigma_W = 8$ km s^{-1}), likely because of peculiar (noncircular) motion of stars. Some Cepheids may be unrecognized members of binary systems.

The measured rotation speed of the Sun Θ_0 is in good agreement with previous determinations. Reid et al. (2014) found $\Theta_0 = 240 \pm 8$ km s^{-1} and $R_0 = 8.34 \pm 0.16$ kpc based on parallaxes and proper motions of high-mass star-forming regions. We measured a slightly smaller velocity of the Sun, but the angular rotation of the Sun about the Galactic center $(\Theta_0 + V_\odot)/R_0 = 30.40 \pm 0.16$ km s^{-1} kpc is similar to that found by Reid et al. (2014): 30.57 ± 0.43 km s^{-1} kpc. Reid & Brunthaler (2004) measured the proper motion of Sagittarius A* of 30.24 ± 0.12 km s^{-1} kpc, which corresponds to $\Theta_0 + V_\odot = 241.9 \pm 1.0$ km s^{-1} for $R_0 = 8$ kpc. The angular velocity of the circular rotation of the Sun ($\Omega_0 = \Theta_0/R_0 = 28.88 \pm 0.31$ km s^{-1} kpc^{-1}) in our model is
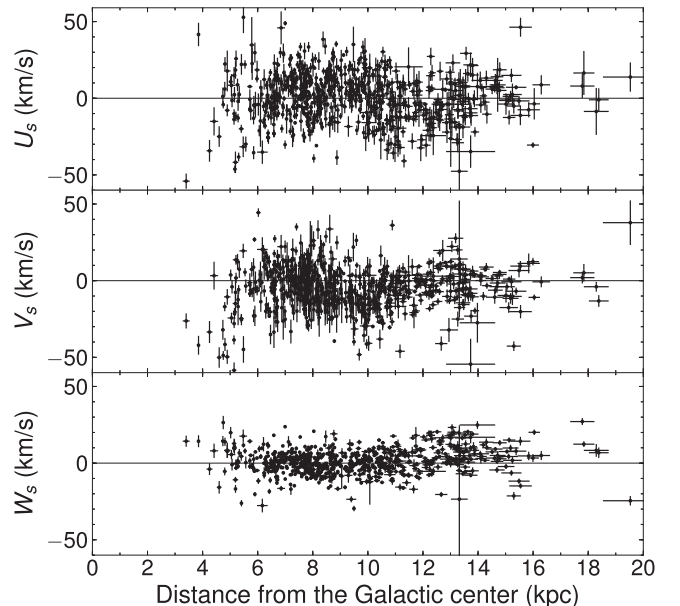
Figure 3. Peculiar (noncircular) motions of Cepheids, after subtracting the model of Galactic rotation (model 2, linear rotation curve). U_s is the velocity component toward the Galactic center, V_s—along the Galactic rotation, and W_s toward the North Galactic pole.

consistent with *Hipparcos* (27.19 ± 0.87 km s^{-1} kpc^{-1}; Feast & Whitelock 1997) and *Gaia* (27.2 ± 0.6 km s^{-1} kpc^{-1}; Bovy 2017) measurements.

4. Galactic Rotation Curve

We use parameters (R_0, Θ_0) from Table 1, model 2 to construct the rotation curve of the Milky Way. We convert radial and tangential heliocentric velocities to the

Galactocentric velocity by adding the motion of the Sun (Equations (5)–(10)). The resulting rotation curve is shown in Figure 2, where we also plotted earlier data from Sofue et al. (2009), rescaled to new (R_0, Θ_0). Both data sets agree well up to a distance of 10–11 kpc from the Galactic center. Previous studies (e.g., Sofue et al. 2009; Russeil et al. 2017) found that the rotation curve outside 12 kpc is nearly constant or even rising (although its precise shape may depend on the choice of R_0 and Θ_0), but these data were affected by large uncertainties and small number of observations (Figure 2). Our rotation curve is nearly flat with a small gradient of -1.34 ± 0.21 km s^{-1} kpc^{-1}, contrary to some earlier claims that the rotation of Cepheids is Keplerian (Gnaciński 2018).

Classical Cepheids are excellent tracers of the rotation curve in the outer parts of the Milky Way disk. Our rotation curve outside 12 kpc is more accurate than in any previous studies (Sofue et al. 2009; Reid et al. 2014) and can be used to constrain the distribution of dark matter in the Milky Way. Currently, our sample includes only 128 Cepheids at Galactocentric distances greater than 12 kpc (out of nearly 600 Cepheids with $R > 12$ kpc from Skowron et al. 2018). Future *Gaia* data releases, as well as a dedicated spectroscopic survey of Cepheids, can provide more accurate insights into rotation of the outer parts of the Milky Way disk.

ORCID iDs

Przemek Mróz ⓘ https://orcid.org/0000-0001-7016-1692
Jan Skowron ⓘ https://orcid.org/0000-0002-2335-1730
Paweł Pietrukowicz ⓘ https://orcid.org/0000-0002-2339-5899
Radosław Poleski ⓘ https://orcid.org/0000-0002-9245-6368
Szymon Kozłowski ⓘ https://orcid.org/0000-0003-4084-880X
Krzysztof Ulaczyk ⓘ https://orcid.org/0000-0001-6364-408X

References

Abuter, R., Amorim, A., Anugu, N., et al. 2018, A&A, 615, L15
Bhattacharjee, P., Chaudhury, S., & Kundu, S. 2014, ApJ, 785, 63
Bovy, J. 2017, MNRAS, 468, L63
Brand, J., & Blitz, L. 1993, A&A, 275, 67
Burton, W. B., & Gordon, M. A. 1978, A&A, 63, 7
Chemin, L., Renaud, F., & Soubiran, C. 2015, A&A, 578, A14
Chu, D. S., Do, T., Hees, A., et al. 2018, ApJ, 854, 12
Clemens, D. P. 1985, ApJ, 295, 422
Durand, S., Acker, A., & Zijlstra, A. 1998, A&AS, 132, 13
Feast, M., & Whitelock, P. 1997, MNRAS, 291, 683
Fich, M., Blitz, L., & Stark, A. A. 1989, ApJ, 342, 272
Foreman-Mackey, D., Hogg, D. W., Lang, D., & Goodman, J. 2013, PASP, 125, 306
Gaia Collaboration, Brown, A. G. A., Vallenari, A., et al. 2018a, A&A, 616, A1
Gaia Collaboration, Katz, D., Antoja, T., et al. 2018b, A&A, 616, A11
Gaia Collaboration, Prusti, T., de Bruijne, J. H. J., et al. 2016, A&A, 595, A1
Gnaciński, P. 2018, arXiv:1809.01951
Groenewegen, M. A. T. 2018, A&A, 619, A8
Honma, M., Nagayama, T., Ando, K., et al. 2012, PASJ, 64, 136
Hron, J. 1987, A&A, 176, 34
Joy, A. H. 1937, ApJ, 86, 363
Kawata, D., Bovy, J., Matsunaga, N., & Baba, J. 2018, MNRAS, 482, 40
McClure-Griffiths, N. M., & Dickey, J. M. 2016, ApJ, 831, 124
McMillan, P. J. 2017, MNRAS, 465, 76
Metzger, M. R., Caldwell, J. A. R., & Schechter, P. L. 1998, AJ, 115, 635
Milgrom, M. 1983, ApJ, 270, 365
Nelder, J. A., & Mead, R. 1965, CompJ, 7, 308
Pato, M., & Iocco, F. 2017, SoftX, 6, 54
Persic, M., Salucci, P., & Stel, F. 1996, MNRAS, 281, 27
Pont, F., Mayor, M., & Burki, G. 1994, A&A, 285, 415
Pont, F., Queloz, D., Bratschi, P., & Mayor, M. 1997, A&A, 318, 416
Reid, M. J., & Brunthaler, A. 2004, ApJ, 616, 872
Reid, M. J., & Dame, T. M. 2016, ApJ, 832, 159
Reid, M. J., Menten, K. M., Brunthaler, A., et al. 2014, ApJ, 783, 130
Reid, M. J., Menten, K. M., Zheng, X. W., et al. 2009, ApJ, 700, 137
Riess, A. G., Casertano, S., Yuan, W., et al. 2018, ApJ, 861, 126
Rubin, V. C., Ford, W. K., Jr., & Thonnard, N. 1980, ApJ, 238, 471
Russeil, D., Zavagno, A., Mège, P., et al. 2017, A&A, 601, L5
Schönrich, R., Binney, J., & Dehnen, W. 2010, MNRAS, 403, 1829
Skowron, D. M., Skowron, J., Mróz, P., et al. 2018, arXiv:1806.10653
Sofue, Y., Honma, M., & Omodaka, T. 2009, PASJ, 61, 227
Stibbs, D. W. N. 1955, MNRAS, 115, 363
Szabados, L. 2003, IBVS, 5394, 1
Udalski, A., Soszyński, I., Pietrukowicz, P., et al. 2018, arXiv:1810.09489
Wang, S., Chen, X., de Grijs, R., & Deng, L. 2018, ApJ, 852, 78